Molecular Vision 2021; 27:61-77 <http://www.molvis.org/molvis/v27/61>
Received 21 August 2020 | Accepted 18 January 2021 | Published 20 January 2021

Effects of topical TGF-β1, TGF-β2, ATX, and LPA on IOP elevation and regulation of the conventional aqueous humor outflow pathway

Natsuko Nakamura,[1,2] Reiko Yamagishi,[1] Megumi Honjo,[1] Nozomi Igarashi,[1] Shota Shimizu,[1,3] Makoto Aihara[1]

[1]Department of Ophthalmology, Graduate School of Medicine, The University of Tokyo, Tokyo, Japan; [2]Division of Vision Research, National Institute of Sensory Organs, National Hospital Organization Tokyo Medical Center, Tokyo, Japan; [3]Senju Laboratory of Ocular Science, Senju Pharmaceutical Co. Ltd., Kobe, Japan

Purpose: The effects of aqueous mediators possibly increasing the outflow resistance, transforming growth factor-β1 (TGF-β1), TGF-β2, autotaxin (ATX), and lysophosphatidic acid (LPA) on human trabecular meshwork (hTM) cells and monkey Schlemm's canal endothelial (SCE) cells were characterized and compared, and the effects of intracameral application of these mediators on intraocular (IOP) elevation were also examined.

Methods: Cells were treated with TGF-β1, TGF-β2, ATX, LPA, or vehicle, and mRNA and protein expression levels of α-SMA, COL1A1, fibronectin, β-catenin, and ZO-1 were examined with real-time quantitative PCR (RT-qPCR) or immunofluorescence analyses or both. The permeability of cell monolayers was measured by determining the transendothelial electrical resistance (TEER) or with the fluorescein isothiocyanate (FITC)-dextran permeability assay. IOP was evaluated in rabbit eyes after intracameral administration of the mediators.

Results: All mediators induced upregulation of α-SMA, COL1A1, and fibronectin in hTM cells. The effect of TGF-β2 on mRNA expression of fibrotic markers was statistically significantly greater than that of TGF-β1. The effects of ATX and LPA indicated the time-dependent difference in the upregulation of α-SMA, COL1A1, and fibronectin. The TEER and FITC-dextran permeability of the SCE cells was evaluated after treatment with TGF-β1 and TGF-β2, but no statistically significant change was observed within 24 h. ATX and LPA also reduced permeability statistically significantly after 3 h and 0.5 h, respectively, and the effect of LPA was more rapid compared to that of ATX. Statistically significant IOP elevation was observed in rabbit eyes as early as 0.5–2.0 h after ATX and LPA treatment and at 24 h after treatment with TGF-β2.

Conclusions: TGF-β2 and ATX and LPA regulate aqueous outflow by modulation of hTM cells and SCE cells, and differences in timing between the effects of each mediator were observed. ATX and LPA showed more rapid effects on IOP elevation than TGF-β2. It was suggested that TGF-β2 and ATX/LPA are involved in increases of IOP, but the timing and sustainability differ between mediators, and they may play specific roles in different glaucoma subtypes.

Elevation of intraocular pressure (IOP) is thought to be derived from increased aqueous humor (AH) outflow resistance mainly located in the conventional pathway [1,2]. The resistance of the conventional pathway involves the trabecular meshwork (TM) and Schlemm's canal (SC) tissues in open angle glaucoma [3]. Cellular responses in the conventional pathway, such as regulation of contractile properties of TM tissue, cytoskeletal and fibrotic changes, cell–cell or cell–matrix interactions in TM cells, the integrity of Schlemm's canal endothelial (SCE) cells, and decreased SC permeability have been suggested to play significant roles in IOP elevation [4-6].

The transforming growth factor (TGF)-β superfamily contributes to a wide variety of cellular processes, including proliferation, differentiation, motility, adhesion, extracellular matrix (ECM) protein synthesis, cancer metastasis, and apoptosis [7]. Among the TGF-β superfamily of growth factors, three genes encode three different TGF-β isoforms (*TGF-β1* [Gene ID 7040, OMIM 190180], *TGF-β2* [Gene ID 7042, OMIM 190220], and *TGF-β3* [Gene ID 7043, OMIM 190230]). These isoforms share 60–80% homology, and all three isoforms activate the same canonical signaling pathway.

Correspondence to: Megumi Honjo, Department of Ophthalmology, Graduate School of Medicine, The University of Tokyo, Tokyo, Japan, 7-3-1 Hongo Bunkyo-ku, Tokyo 1138655, Japan; email: honjomegumi@gmail.com

It has been reported that they appear to have similar functions in vitro, but studies with knockout mice for all isoforms have suggested that each isoform may play a different role in vivo [8]. TGF-β2 is elevated in the AH of patients with primary open angle glaucoma (POAG), the most common form of glaucoma, and is thought to be an important contributor to the pathogenesis of glaucoma. TGF-β2 is the most abundant TGF-β isoform in the eye, and TGF-β2 influences many aspects of cellular behavior, including proliferation, differentiation, migration, and ECM synthesis and breakdown [9-11]. In glaucoma pathogenesis, TGF-β2 increases AH resistance by upregulation of ECM components, such as fibronectin, collagen I (COL1A1), collagen IV (COL4A1), and regulation of changes in the epithelial mesenchymal transition (EMT) in TM cells, resulting in fibrotic changes in the TM related to the pathogenesis of POAG [12-14].

We previously reported that the AH level of lysophosphatidic acid (LPA) and autotaxin (ATX), an enzyme involved in the generation of LPA by lysoPLD activity, was upregulated in open angle glaucoma, particularly in secondary open angle glaucoma (SOAG) and exfoliation glaucoma (XFG), in which aqueous TGF-β2 was downregulated [15,16]. LPA is a simple phospholipid but induces many types of cellular responses, including Rho GTPase–regulated cell adhesion, contraction, cellular proliferation, cell migration, cytokine and chemokine secretion, platelet aggregation, transformation of smooth muscle cells, and neurite retraction [17]. ATX is a secreted glycoprotein, widely present in biologic fluids, including serum and aqueous humor [16,18]. Previously, we reported that upregulation of the ATX/LPA pathway was statistically significantly positively correlated with IOP elevation. We also confirmed that ATX was induced in human TM (hTM) cells with dexamethasone (Dex) treatment and induced a fibrotic response and production of ECM components, such as fibronectin, COL1A, and COL4A, in hTM cells in an autocrine and paracrine manner, which, in turn, led to fibrotic changes in the tissue [15]. These results explain the upregulation of the ATX/LPA pathway-induced impediment of AH outflow through the TM and the increase in IOP. LPA has been shown to increase resistance to AH outflow through TM fibrosis based on the observation that the perfusion of LPA lowered outflow facility in ex vivo human ocular organ culture of the anterior segment of the eye or LPA-induced fibrosis or increased production of the ECM in hTM cells in vitro [19-21]. However, there have been no studies to determine whether exogenous application of LPA or ATX can affect IOP in vivo. In addition, we recently found that TGF-β1, TGF-β2, and ATX were differentially upregulated in a glaucoma subtype-specific manner in AH, but to the best of our knowledge, there have been no comparative studies on the effects of these mediators on hTM cells or SCE cells. It has been suggested that TGF-β2 plays a leading role in the pathogenesis of glaucoma, while TGF-β1 has also been suggested to be involved in fibrotic changes associated with AH outflow. However, the details of the differences between these TGF-β isoforms with regard to their roles in regulation of AH outflow remain unclear.

We hypothesized that there may be differences in the effects of TGF-β1, TGF-β2, and ATX/LPA on hTM cells and SCE cells, which may be related to the IOP elevation profiles of different glaucoma subtypes. Therefore, in the present study we investigated the effects of these mediators on fibrotic responses in hTM cells and SCE permeability. We also confirmed the characteristic IOP elevation after topical application of TGF-β2 and ATX/LPA.

METHODS

Cell culture:

Preparation and characterization of hTM cell culture and treatment—Primary hTM cells were isolated from human donor eyes and characterized as described previously, according to the recommendations of Keller et al. [22]. Only well-characterized normal hTM cells, in which Dex-induced myocilin upregulation was confirmed with quantitative real-time polymerase chain reaction (RT-qPCR) from passages 3 through 5 were used for subsequent studies (Figure 1). The hTM cells from three donor eyes (46 years old, 52 years old, and 55 years old, without glaucoma) were used in this study. For further hTM cell characterization, western blotting for Dex-induced myocilin upregulation and immunocytochemistry using antibodies against AQP-1, vimentin, TIMP-3, and desmin was performed according to previous reports [23,24]. All in vitro experiments were performed 24 h after confluence was confirmed. After overnight serum starvation, the cells were treated with 1, 10 ng/ml TGF-β1, TGF-β2, 40 μM ATX, or 1, 10 μM LPA with or without the ROCK inhibitor (10 μM K115; Kowa, Nagoya, Aichi, Japan) which inhibit the downstream cascade of TGF-β and the ATX/LPA pathway, ATX inhibitor (10 μM HA130; Merck, Kenilworth, NJ), or LPA receptor (LPAR) antagonist (10 μM Ki16425; Merck) and TGF-β inhibitor (10 μM SB431542; Fujifilm, Osaka, Japan). Each experiment was performed at least three times, and the consistency of experiment was confirmed using biologic triplicates.

Culture of monkey Schlemm's canal endothelial cells—SCE explants dissected from the eyes of 6- to 12-month-old non-glaucomatous cynomolgus monkeys were obtained from a commercial laboratory (Shin Nippon Biomedical Laboratories, Kagoshima, Japan). We modified

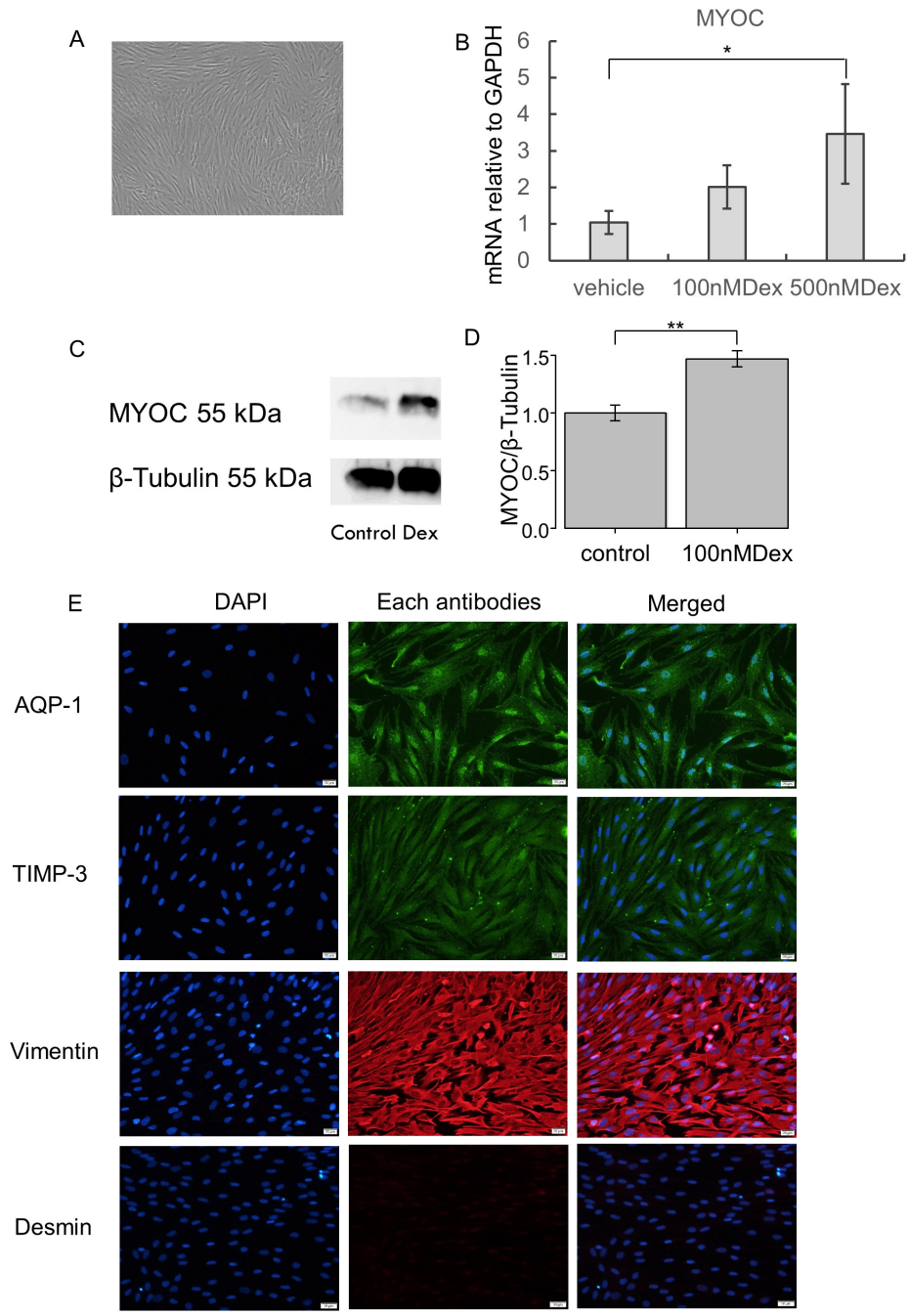

Figure 1. Characterization of hTM cells. **A**: The image of human trabecular meshwork (hTM) cells using a contrast-phase microscope. **B**: The statistically significantly increased mRNA expression of myocilin was confirmed with 500 nM dexamethasone (Dex) treatment (7 days). *p<0.05. **C**, **D**: Upregulation of myocilin was also confirmed with western blotting in hTM cells stimulated with 100 nM Dex. **C**: The representative bands for western blotting. **D**: The relative expression of myocilin to the loading control of β-tubulin (n = 3). **p<0.01. **E**: The panels show cells stained for 4',6-diamidino-2-phenylindole (DAPI; blue), endothelial cell markers, and mesenchymal markers, merged images from left to right. The hTM cells used in the study were positive for AQP-1, TIMP-3, and vimentin, but were negative for desmin. Bar, 200 µm.

Alvarado et al.'s dissection methods [25-27]. At least three cell lines of SCE cells from three monkey eyes were used in the study. Primary SCE cells were cultured in Dulbecco's modified Eagle's medium (DMEM) containing 10% fetal bovine serum (FBS) and antibiotic antimycotic solution (100X; Sigma-Aldrich, St. Louis, MO) at 37 °C in 5% CO_2. SCE cells between passages 4 and 6 were used in all experiments.

RNA extraction and RT-qPCR—To measure fibrotic changes and ECM gene expression, and to characterize hTM cell strain profiles in hTM cells, RT-qPCR was performed as described previously [15,28]. Confluent cultures of hTM cells that had been starved of serum for 24 h were treated with mediators and inhibitors or antagonists and subjected to RT-qPCR. For characterization, the cells were treated with 100 nM or 500 nM Dex for 7 days without serum starvation. The cells were lysed using TRI Reagent (Molecular Research Center, Inc., Cincinnati, OH), and mRNA was isolated using chloroform and isopropyl alcohol as previously described [15,28]. mRNA was treated with a PrimeScript RT Reagent Kit (Takara Bio, Shiga, Japan) to synthesize cDNA. mRNA was quantified using quantitative PCR (qPCR) with SYBR Premix Ex TaqII (Tli RNaseH Plus; Takara Bio) and the Thermal Cycler Dice Real Time System II (Takara Bio) using the ΔΔCt method. For qPCR, primer sequences were taken from previously published sequences, and the primers were purchased from Hokkaido System Science (Hokkaido, Japan). The sequences of PCR primers used are described in Table 1. Target gene expression was normalized relative to that of *GAPDH* mRNA. All tests were conducted in triplicate to ensure reproducibility, and the consistency of the experiment was confirmed using biologic triplicates.

Western blotting: Western blotting was performed as described previously [15,28]. Confluent cultures of hTM cells that had been starved of serum for 24 h were treated with or without 100 nM Dex. After 1 dpi, the cells were collected in radioimmunoprecipitation assay (RIPA) buffer (Thermo Fisher Scientific) containing protease inhibitors (Roche Diagnostics, Basel, Switzerland), sonicated, and centrifuged. After protein concentrations in the supernatant were determined by the bicinchoninic acid assay, using a BCA Protein Assay Kit (Thermo Fisher Scientific K.K.), sodium dodecyl sulfate–polyacrylamide gel electrophoresis (SDS–PAGE) were performed as previously described [28]. Protein bands were transferred to polyvinylidene difluoride (PVDF) membranes (Bio-Rad Laboratories, Hercules, CA), and the membranes were immersed in Tris-buffered saline with Tween-20 (TBST) containing primary antibody. After washing, the membranes were immersed in TBST containing secondary antibody and reacted with enhanced chemiluminescent (ECL) substrate (Thermo Fisher Scientific). Protein bands were detected with ImageQuant LAS 4000 mini (GE Healthcare, Chicago, IL). The primary antibodies were anti-myocilin (NT) antibody, clone 7.1 (1:1,000; Merck Millipore, Billerica, MA) and anti-β-tubulin (1:1,000; Wako Pure Chemical Industries, Ltd., Osaka, Japan), and horseradish peroxidase (HRP)–conjugated secondary antibody (1:2,000; Thermo Fisher Scientific). The membrane was stripped with WB Stripping Solution (nacalai tesque, Kyoto, Japan) and reblotted. The bands were quantified using ImageJ software (ver. 1.49, NIH, Bethesda, MD).

Immunocytochemistry: Immunocytochemistry was performed as described previously [15,28]. The primary antibodies were anti-α-SMA (1:500; Dako, Agilent, Santa Clara, CA), anti-fibronectin (1:400; Santa Cruz Biotechnology, Dallas, TX), rhodamine phalloidin (0.2 μM; Thermo Fisher Scientific, Waltham, MA), anti-ATX (1:200; MBL, Nagoya, Japan), anti-COL1A1 (1:200; Rockland Immunochemicals, Limerick, PA), anti-AQP-1 antibody (1:500; Santa Cruz Biotechnology, Inc., Santa Cruz, CA), anti-vimentin antibody (1:1,000; Abcam, Cambridge, MA), anti-desmin antibody (1:200; Abcam), and anti-TIMP-3 antibody (KYOWA PHARMA CHEMICAL, CO., LTD, Toyama, Japan). Alexa

Table 1. PCR information.

Gene	Primer	
	Forward (5'-3')	**Reverse (5'-3')**
GAPDH	GAGTCAACGGATTTGGTCGT	TTGATTTTGGAGGGATCTCG
ATX	ACAACGAGGAGAGCTGCAAT	AGAAGTCCAGGCTGGTGAGA
fibronectin	AAACCAATTCTTGGAGCAGG	CCATAAAGGGCAACCAAGAG
COL1A1	CAGCCGCTTCACCTACAGC	TTTTGTATTCAATCACTGTCTTG
COL4A1	TAGAGAGGAGCGAGATGTTC	GTGACATTAGCTGAGTCAGG
αSMA	CCGACCGAATGCAGAAGGA	ACAGAGTATTTGCGCTCCGAA
Myocilin	TACACGGACATTGACTTGGC	ATTGGCGACTGACTGCTTAC

Fluor 488 and Alexa Fluor 594 secondary antibodies (1:1,000) were purchased from Thermo Fisher Scientific. The slides were imaged under a fluorescence microscope (BZ-9000; Keyence, Osaka, Japan).

Measurement of monolayer cell permeability and TEER: Measurements of the monolayer transendothelial electrical resistance (TEER) and the permeability of the SCE cells were performed as described previously [25,26,28,29]. After overnight serum starvation, the SCE cells were treated with 10 ng/ml TGF-β1, 10 ng/ml TGF-β2, 40 μM ATX, or 10 μM LPA with or without inhibitors. The concentration of 4 kDa fluorescein isothiocyanate (FITC)-dextran (Sigma-Aldrich) was measured 1, 3, 6, and 24 h after the tracer was added using a multimode plate reader (Multi Microplate Reader, MTP-800AFC; Corona Electric, Ibaragi, Japan) with an excitation wavelength of 490 nm and an emission wavelength of 530 nm, and the same volume of the culture medium was added to replace the medium removed. The TEER was measured 1, 3, and 6 h after stimulation. Each experiment was performed at least four times.

Animal experiments and IOP measurement: All animals used in this study were treated in accordance with the ARVO Statement for the Use of Animals in Ophthalmic and Vision Research and the dictates of the Institutional Animal Research Committee of the University of Tokyo. Five male Japanese white rabbits (average weight 2.5 kg, 9 to 12 months old) were used. The animals were maintained in conventional animal rooms and housed in individual plastic cages in an air-conditioned room with a temperature of 22 °C ± 3.0 °C, 55% ± 10% relative humidity, and a 12 h:12 h light-dark cycle, with access to food and water ad libitum. The rabbits were acclimated for 2 weeks before use in the experiments. IOP was measured with Pneumatonometer Model 30 Classic (RE Medical Inc., Osaka, Japan) under topical anesthesia with 0.4% oxybuprocaine hydrochloride eye drops in a single-blind comparative study of four regimens with a single drop for one eye. The rabbits received intracameral administration of 30 μl TGF-β2 (100 ng/ml), ATX (400 μM), or LPA (100 μM) diluted with PBS (1X; 120 mM NaCl, 20 mM KCl, 10 mM, $NaPO_4$, 5 mM KPO_4, pH 7.4) in one eye. The other eye was treated with intracameral administration of the same volume of PBS and used as a control. A microsyringe with a 30 G needle (Terumo Corporation, Tokyo, Japan) was used for the intracameral injections, and it was confirmed that there was no leakage after each injection. The rabbits were put under sedation with medetomidine (20 μg/kg, i.m., Nippon Zenyaku Kogyo Co., Ltd., Fukushima, Japan), and the sedation was antagonized and reversed with atipamezole (100 μg/kg, i.m., Nippon Zenyaku Kogyo Co., Ltd.) immediately after the injection. The IOP was measured after the confirmation that rabbits were completely awake and could eat and drink. The target AH concentrations were calculated as 10 ng/ml TGF-β2, 40 μM ATX, and 10 μM LPA based on the estimated volume of 300 μl for the rabbit anterior chamber. The concentration of each mediator was set based on the in vitro study. One of the researchers (NI) randomly allocated the regimen for each group, and the examiners were all blinded to the allocated regimens. Each regimen was performed with 2-week intervals as washout periods, and the baseline IOP was remeasured and confirmed. Three IOP measurements were obtained, and the average difference in IOP between the treated eye and the control eye was recorded.

Statistical analyses: Statistical analyses were performed with JMP Pro 15 software (SAS Institute Inc., Cary, NC). The results are expressed as the mean ± standard deviation (SD). Differences in the data among the groups were analyzed with analysis of variance (ANOVA) and Tukey's post hoc test. For the IOP measurement of rabbit eyes, a repeated-measures ANOVA was used. In all analyses, a p value of less than 0.05 was considered statistically significant.

RESULTS

Characterization of hTM cells: We characterized hTM cells in accordance with the previous reports [22-27]. Figure 1A shows the representative image of hTM cells using a contrast-phase microscope. Statistically significant upregulation of mRNA expression of myocilin was confirmed with RT-qPCR with the Dex treatment (Figure 1B). Western blotting also indicated that the protein expression of myocilin was upregulated when stimulated with the Dex treatment. The quantitative analysis showed that the expression of myocilin was statistically significantly upregulated by the Dex treatment (Figure 1C,D). We performed immunocytochemistry to characterize the hTM cells, and the hTM cells were confirmed to be positive for AQP-1, vimentin, and TIMP-3, but were negative for desmin (Figure 1E).

Effects of TGF-β1 and TGF-β2 on expression of fibrogenic markers and cytoskeletal proteins in hTM cells

First, we analyzed the effects of exogenous TGF-β1 and TGF-β2 on the protein and mRNA expression of the fibrogenic markers and cytoskeletal proteins in the hTM cells with immunocytochemistry and RT-qPCR. As shown in Figure 2, treatment with 10 ng/ml TGF-β1 and TGF-β2 for 24 h induced changes in the distribution of F-actin and upregulation of α-SMA protein expression, both of which were attenuated with treatment with the TGF-β inhibitor and the ROCK inhibitor. RT-qPCR showed that the level of α-SMA mRNA expression was statistically significantly upregulated

by TGF-β1 and TGF-β2 compared to the control, but there was a statistically significant difference between the effects of TGF-β1 and TGF-β2 (Figure 3). With regard to the fibrogenic markers, TGF-β2 induced fibronectin and COL1A1 protein and mRNA expression compared to the control, and the TGF-β inhibitor and the ROCK inhibitor attenuated the upregulation of these fibrogenic markers (Figure 2, Figure 3). TGF-β1 tended to upregulate the expression of the fibrogenic markers, but the effects were not statistically significant (Figure 3). To compare the effects of two different isoforms of TGF-β, we compared the fibrogenic effects of those mediators on hTM cells at 6 and 24 h post-stimulation to identify

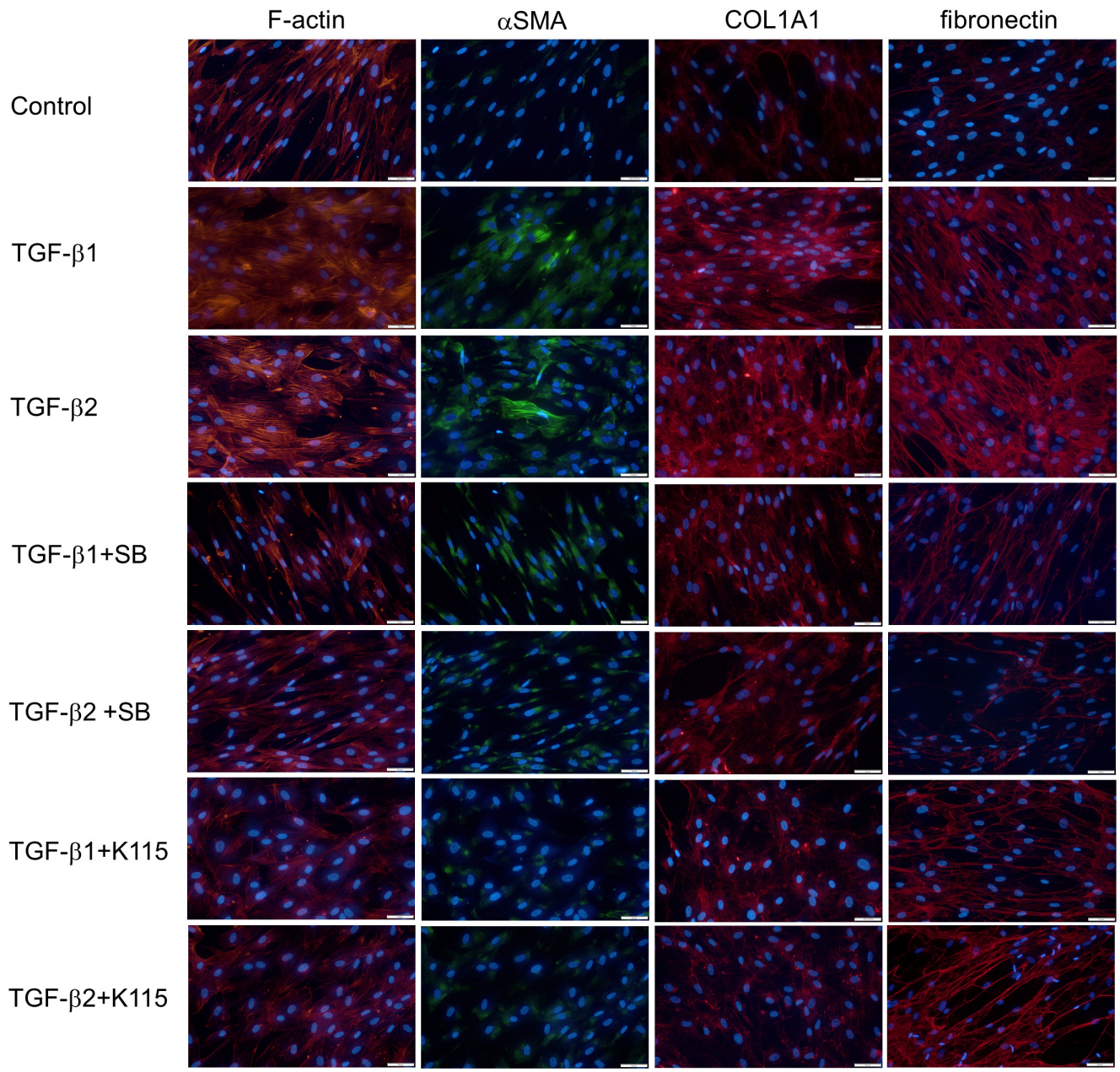

Figure 2. Immunocytochemistry of F-actin, α-SMA, COL1A1, and fibronectin in hTM cells treated with TGF-β1 and TGF-β2. The human trabecular meshwork (hTM) cells were treated with 10 ng/ml of TGF-β1 and TGF-β2 for 24 h with or without the TGF-β inhibitor or the ROCK inhibitor. The panels show cells stained for F-actin (red), α-SMA (green), COL1A1 (red), and fibronectin (red) merged with 4',6-diamidino-2-phenylindole (DAPI; blue) from left to right. The expression of F-actin was altered, and the expression of α-SMA, COL1A1, and fibronectin was increased by TGF-β1 and TGF-β2; these effects were attenuated by the TGF-β inhibitor or the ROCK inhibitor. Bar, 200 µm.

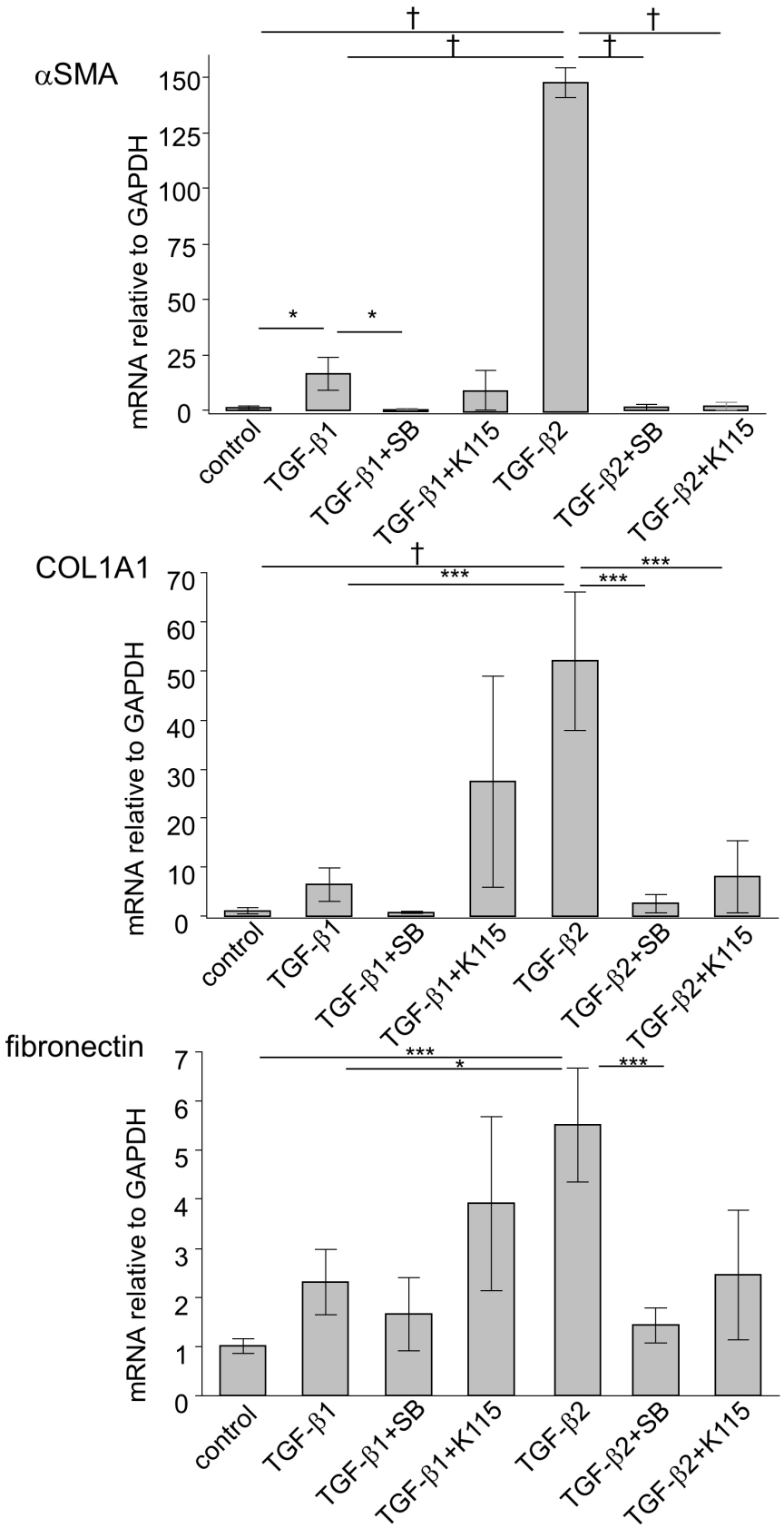

Figure 3. RT-qPCR quantification of TGF-β1 and TGF-β2-induced fibrotic changes in hTM cells α-SMA, COL1A1, and fibronectin mRNA expression were statistically significantly induced with 10 ng/ml TGF-β2 treatment (24 h). With the exception of fibronectin, these effects were statistically significantly attenuated by the TGF-β inhibitor or the ROCK inhibitor. TGF-β1 (10 ng/ml, 24 h) induced statistically significant increased expression of only α-SMA, but not COL1A1 or fibronectin. Real-time quantitative PCR (RT-qPCR) was performed with *GAPDH* primers as an internal control for input DNA. Data are the averages of four independent samples. Values are the mean ± standard deviation. *p<0.05, **p<0.01, ***p<0.001, †p<0.0001.

the difference among different concentrations using immunocytochemistry (Figure 4). The upregulation of expression of α-SMA and fibronectin after treatment with each TGF-β isoform was confirmed to be dose dependent, and the effects of 10 ng/ml TGF-β1 were comparable to those of 1 ng/ml TGF-β2.

Effects of TGF-β1 and TGF-β2 on monolayer permeability and molecules associated with cell–cell contact in SCE cells: The upregulation of the flux of FITC-dextran reflects the increased permeability, and increased TEER reflects the lowering permeability. Permeability assays using the flux of FITC-dextran as an indicator showed that treatment with TGF-β1 or TGF-β2 had no statistically significant effect on the concentration of FITC-dextran on the apical side at 1, 3, 6, and 24 h (Figure 5A). Additional treatment with the TGF-β inhibitor did not statistically significantly alter the concentration of FITC-dextran, suggesting that neither TGF-β1 nor TGF-β2 affected SCE permeability more or less, at least within 24 h. Immunocytochemical staining revealed modest upregulation of tight junction-related proteins, such

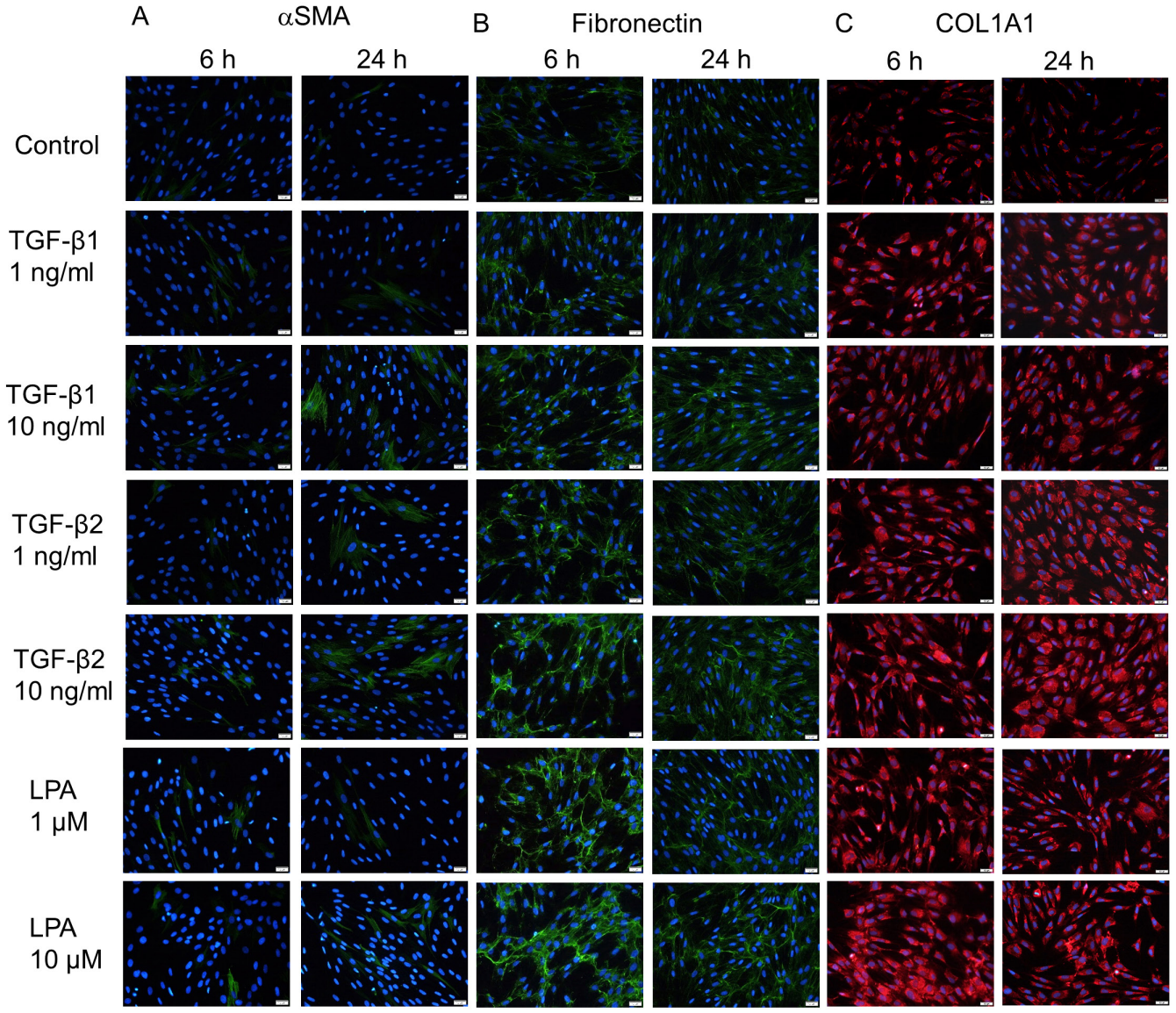

Figure 4. Immunocytochemistry of α-SMA, COL1A1, and fibronectin in hTM cells treated with TGF-β1, TGF-β2, and LPA. The human trabecular meshwork (hTM) cells were treated with 10 ng/ml of TGF-β1 and 1 ng/ml TGF-β2 or 1 or 10 μM lysophosphatidic acid (LPA) for 6 and 24 h. The panels show cells stained for α-SMA (green, **A**), fibronectin (green, **B**), and COL1A1 (red, **C**) merged with 4',6-diamidino-2-phenylindole (DAPI; blue). Bar, 200 μm.

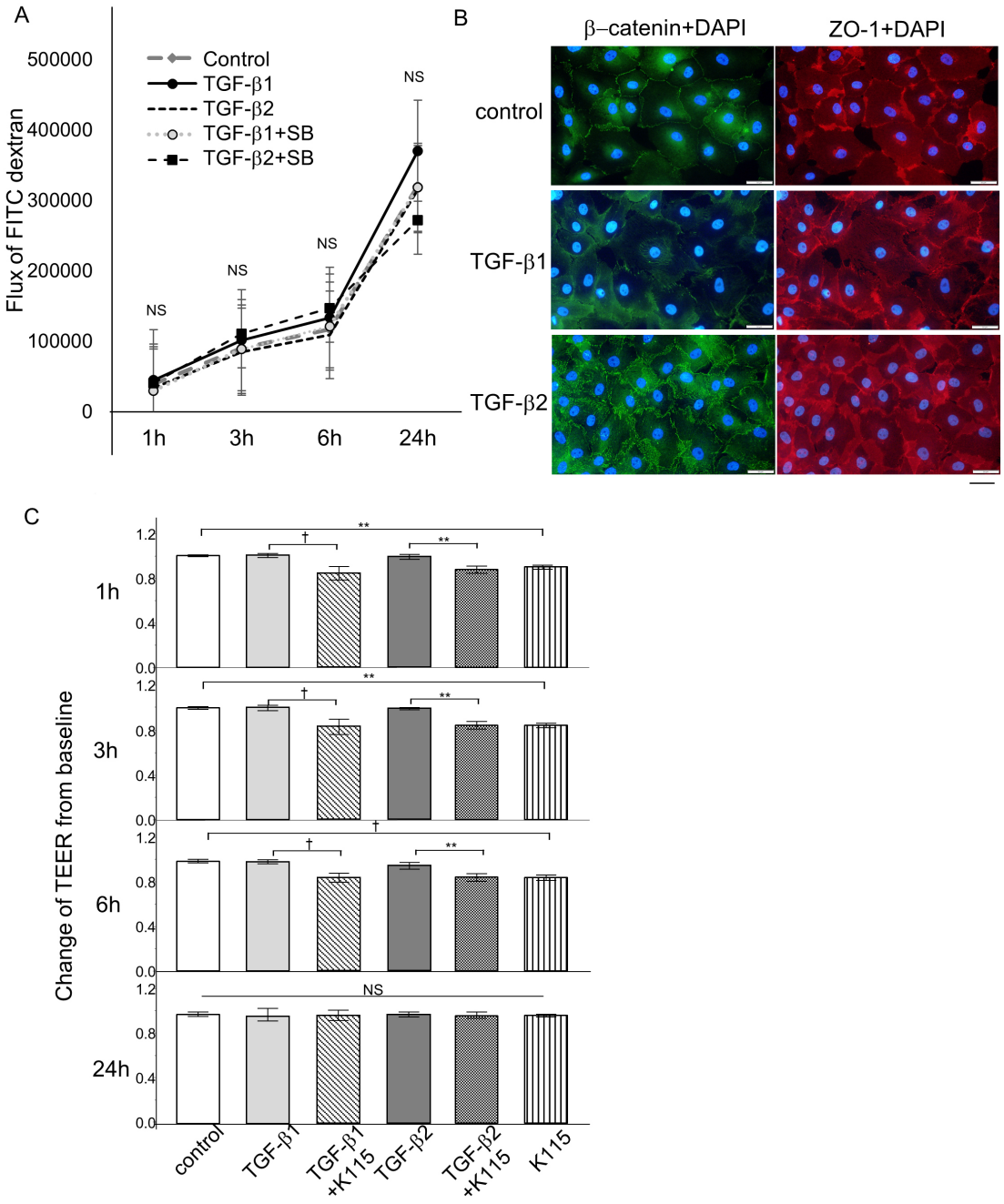

Figure 5. Effects of TGF-β1 and TGF-β2 on monolayer permeability and TEER, and molecules associated with cell–cell contact in SCE cells. **A**: Changes in Schlemm's canal endothelial (SCE) cell monolayer permeability using 4 kDa fluorescein isothiocyanate (FITC)-dextran are shown. SCE cells were exposed to TGF-β1 or TGF-β2 with or without the TGF-β inhibitor, and the concentrations of FITC-dextran were measured at 1, 3, 6, and 24 h after treatment. No statistically significant differences were observed between the control and treated cells within 24 h. **B**: Immunocytochemistry in SCE cells treated with 10 ng/ml TGF-β1 or TGF-β2 after 24 h. The left panels show staining for β-catenin (green), and the right panels show staining for ZO-1 (red) merged with 4',6-diamidino-2-phenylindole (DAPI; blue). β-catenin and ZO-1 expression increased after treatment. Bar, 200 µm. **C**: The transendothelial electrical resistance (TEER) measured in SCE cells exposed to TGF-β1 or TGF-β2 with or without the ROCK inhibitor at 1, 3, 6, and 24 h after treatment. There were no statistically significant changes in the TEER induced by TGF-β1 or TGF-β2 compared to the control within 24 h, although the ROCK inhibitor statistically significantly decreased the TEER at 1, 3, and 6 h. Values are the mean ± standard deviation. *p<0.05, **p<0.01, ***p<0.001, †p<0.0001.

as ZO-1, in the TGF-β1- and TGF-β2-treated cells (Figure 5B). Staining for β-catenin, a molecule related to adherens junctions, also tended to be upregulated after treatment with TGF-β1 and TGF-β2, but the changes were not statistically significant. To confirm the results of FITC-dextran flux and immunocytochemical staining in SCE cells, we measured the TEER. The TEER of the SCE cell monolayer after TGF-β1 and TGF-β2 were added did not show any statistically significant differences from the control at 1, 3, 6, and 24 h (Figure 5C). Interestingly, the TEER values were statistically significantly different when TGF-β1 or TGF-β2 was added concomitant with the ROCK inhibitor, K115, at 1, 3, and 6 h. The values were not statistically significantly different among the samples even when treated with K115 at 24 h.

Effects of the ATX/LPA pathway on expression of fibrogenic markers and cytoskeletal proteins in hTM cells: Next, we investigated the effects of exogenous ATX and LPA on protein and mRNA expression of fibrogenic markers and cytoskeletal proteins in hTM cells as well as with immunocytochemistry and RT-qPCR. As shown in Figure 6, ATX and LPA induced upregulation of α-SMA protein expression (Figure 6A) and changes in the distribution of F-actin (Figure 6B), and the upregulation of α-SMA was attenuated by the ATX inhibitor, the LPAR antagonist, and the ROCK inhibitor treatment. LPA showed more rapid effects on α-SMA protein upregulation than ATX (Figure 6B), which was also confirmed with RT-qPCR (Figure 7). When compared at 6 h, the effect of LPA on α-SMA protein upregulation was stronger than that of ATX; however, the effects of LPA and ATX were almost identical concerning fibronectin upregulation. As shown in Figure 4, the effect of LPA was dose dependent, and 10 μM LPA showed more rapid effects on α-SMA protein upregulation than 10 ng/ml TGF-β2. The ROCK inhibitor, the ATX inhibitor, and the LPAR antagonist attenuated the ATX- and LPA-induced changes in α-SMA upregulation (Figure 6). With regard to the fibrogenic markers, ATX and LPA induced upregulation of COL1A1 protein expression (Figure 6A), which was attenuated by the ATX inhibitor, the LPAR antagonist, or the ROCK inhibitor. We also observed a difference in the timing of the effects of ATX and LPA on COL1A1 expression; LPA upregulated COL1A1 as early as 3 h, whereas the effect of ATX was seen after 6 h. The difference in the timing of the effects between ATX and LPA was also confirmed with RT-qPCR (Figure 7). Fibronectin upregulation was observed following ATX or LPA treatment with immunocytochemistry, and RT-qPCR also showed statistically significant upregulation at 1 h after ATX treatment (Figure 7). However, the expression was not that prominent compared to that of the control, and there was no statistically significant upregulation of fibronectin mRNA at 6 and 24 h (Figure 7).

Effects of the ATX/LPA pathway on TEER and molecules associated with cell–cell contact in SCE cells: The TEER of the SCE cell monolayer after ATX was added was statistically significantly higher than that of the controls at 1, 3, and 6 h, and treatment with the ATX inhibitor attenuated the increase in the TEER to a value comparable to that for controls (Figure 8A). Treatment with the ROCK inhibitor statistically significantly reduced the increased TEER induced by ATX. The TEER of the SCE cell monolayer after LPA was added was statistically significantly higher than that of controls at 0.5, 1, and 3 h, and treatment with the LPAR antagonist attenuated the increase in the TEER to a value comparable to that for the controls (Figure 8B). Treatment with the ROCK inhibitor also statistically significantly reduced the increased TEER induced by LPA. We found differences in the timing of the effects between ATX and LPA, as LPA showed more rapid effects on SCE permeability compared to ATX. Immunocytochemical staining revealed robust rearrangement of F-actin and upregulation of the tight junction-related protein, ZO-1, in the ATX- and LPA-treated cells (Figure 8C). Staining of the adherens junction-related molecule, β-catenin, was also increased after treatment with ATX and LPA. The ATX inhibitor or the LPAR antagonist attenuated the F-actin rearrangement and ZO-1 upregulation, and β-catenin tended to show a broad and sparse expression pattern after treatment with the ROCK inhibitor (Figure 8C).

Effects of intracameral ATX, LPA, and TGF-β2 on intraocular pressure in rabbit eyes: IOP was measured after intracameral instillation of ATX, LPA, and TGF-β2 (Figure 9). We did not perform the instillation of TGF-β1 because the effect of TGF-β1 was limited and not statistically significant in the in vitro study with hTM cells and SCE cells. LPA induced statistically significant IOP elevation compared to controls from 0.5 h after instillation, which persisted until 1.5 h. ATX also induced statistically significant IOP elevation with an increase of up to 6 mmHg from 1 to 2 h. TGF-β2 did not show any statistically significant effect on IOP until 24 h, but induced statistically significant IOP elevation with an increase of up to 4 mmHg at 24 h. However, the IOP at 48 h was not statistically significantly different from that for the controls.

DISCUSSION

We compared the effects of mediators that are involved in the pathogenesis of glaucomatous changes in the AH pathway and IOP elevation using TM cells and SCE cells in vitro and rabbit eyes in vivo. The effects of TGF-β1, TGF-β2, ATX, and

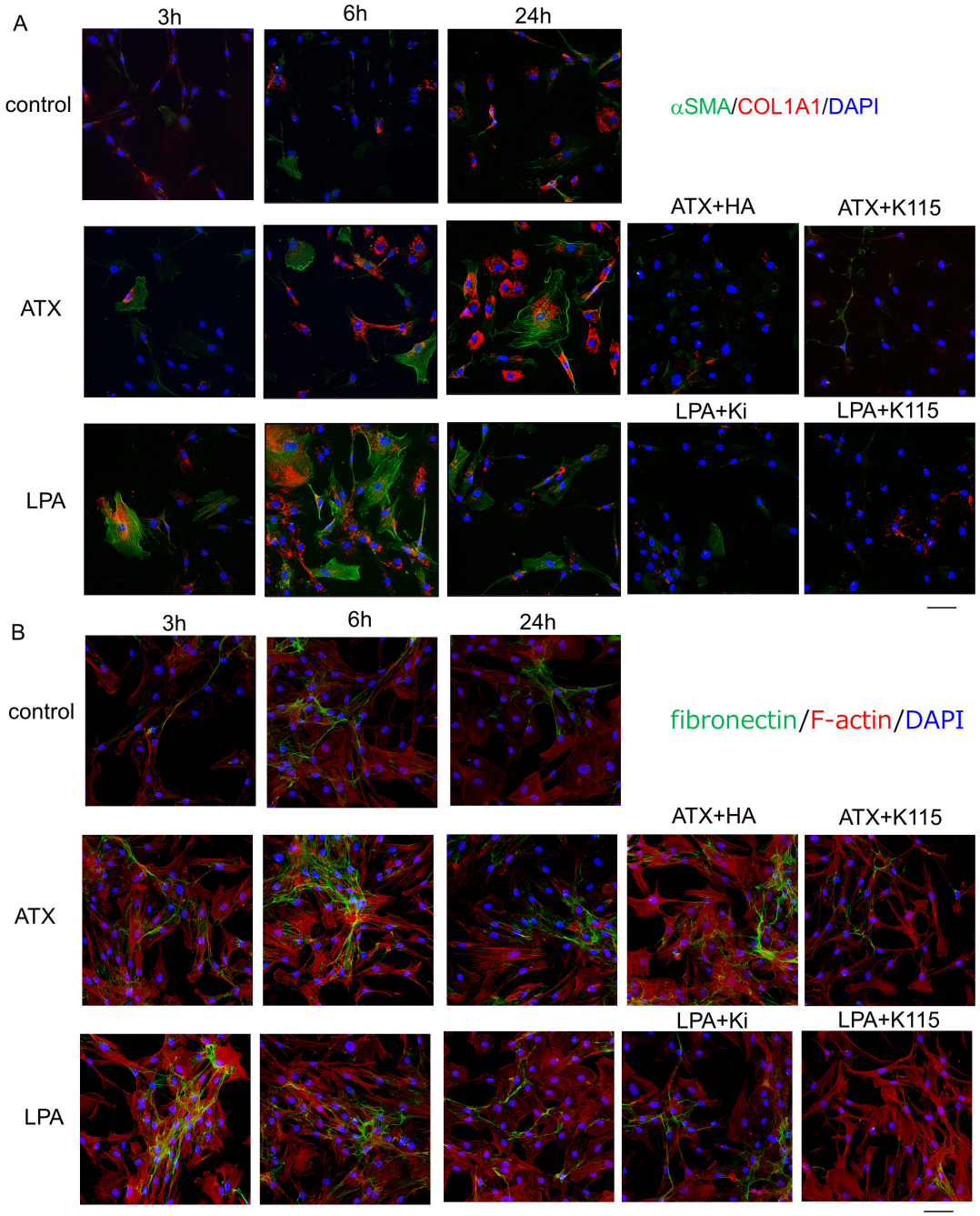

Figure 6. Immunocytochemistry for F-actin, α-SMA, COL1A1, and fibronectin in hTM cells treated with ATX and LPA. **A**: Immunostaining for α-SMA (green) and COL1A1 (red) merged with 4',6-diamidino-2-phenylindole (DAPI; blue) at 3, 6, and 24 h after treatment with 40 µM autotaxin (ATX) or 10 µM lysophosphatidic acid (LPA). LPA induced upregulation of α-SMA or COL1A1 from 3 h after treatment, and ATX induced upregulation of α-SMA or COL1A1 from 6 h after treatment. The ATX inhibitor, the LPAR antagonist, and the ROCK inhibitor statistically significantly attenuated these changes. **B**: Immunostaining for fibronectin (green) and F-actin (red) merged with DAPI (blue) at 3, 6, and 24 h after treatment with ATX or LPA. LPA and ATX induced upregulation of fibronectin from 3 h after treatment, and the ATX inhibitor, the LPAR antagonist, and the ROCK inhibitor attenuated these changes. Bar, 200 µm.

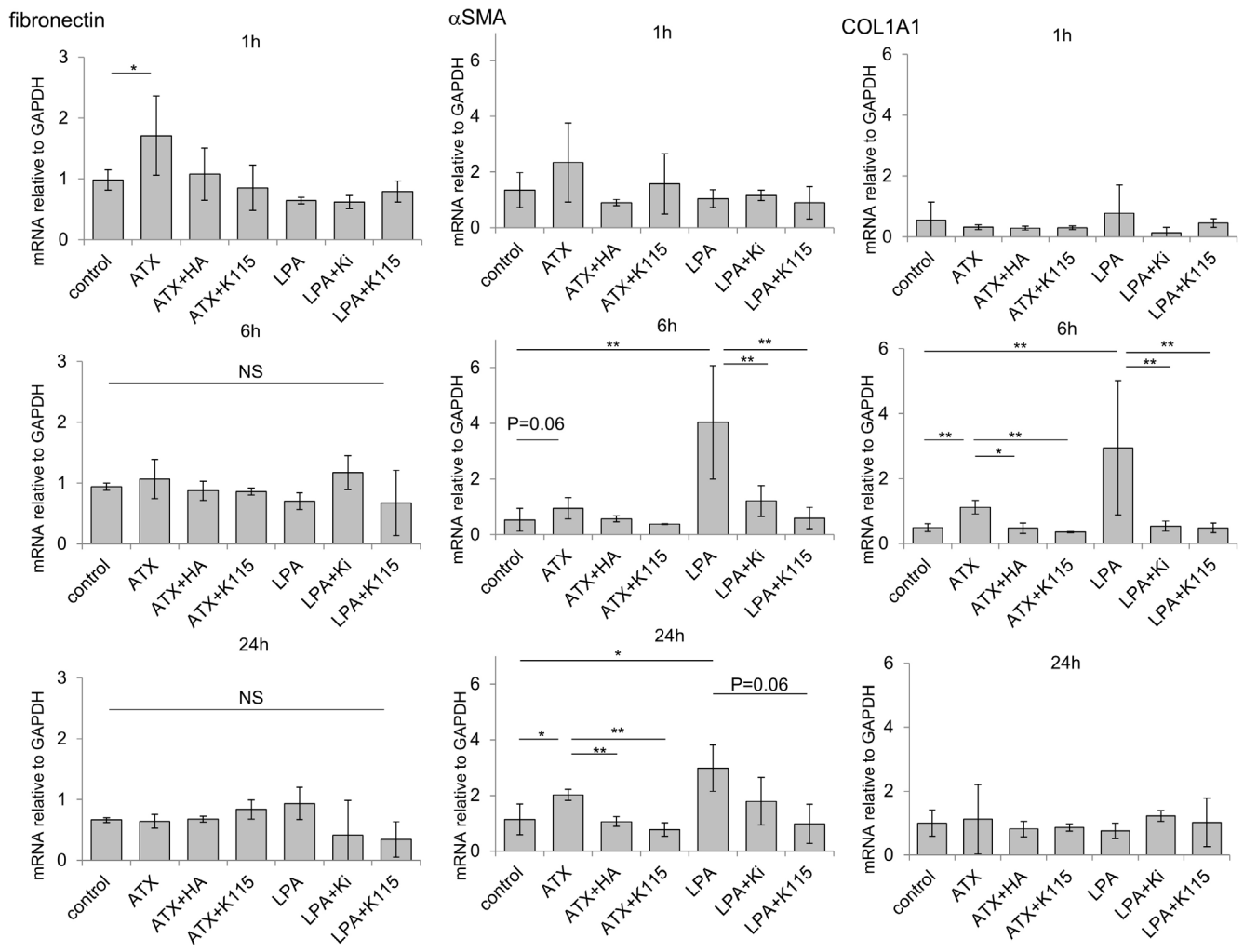

Figure 7. RT-qPCR quantification of TGF-β1- and TGF-β2-induced fibrotic changes in the α-SMA, COL1A1, and fibronectin mRNA expression of hTM cells at 1, 6, and 24 h after ATX and LPA treatment are shown. α-SMA was statistically significantly induced by lysophosphatidic acid (LPA; 6 h, 24 h) and autotaxin (ATX; 24 h), and these effects were statistically significantly attenuated by the LPAR antagonist, ATX inhibitor, or ROCK inhibitor. COL1A1 was statistically significantly induced by LPA (6 h) and ATX (6 h), and these effects were statistically significantly attenuated by the LPAR antagonist, ATX inhibitor, or ROCK inhibitor. ATX was upregulated by ATX (1 h). Real-time quantitative PCR (RT-qPCR) was performed with *GAPDH* primers to serve as an internal control for input DNA. Values are the mean ± standard deviation of four independent samples. *p<0.05, **p<0.01, ***p<0.001, †p<0.0001.

LPA on TM fibrosis, SCE permeability, and IOP elevation were examined. We found statistically significant differences in the effects of these mediators, particularly with regard to their timing, which may reflect the characteristic upregulation of these mediators in glaucoma subtypes.

IOP is regulated by the resistance of conventional outflow through the TM and Schlemm's canal, and some studies have suggested that the profiles of cytokines in the AH are associated with changes in the aqueous pathway [30-32]. Among the various cytokines examined, elevated levels of TGF-β2 were found in the glaucomatous AH, particularly in POAG, in several previous studies, including ours [33-35]. TGF-β2 has been suggested to play critical roles in the pathogenesis of POAG based on elevated levels in the AH of POAG and its ability to induce ECM remodeling and TM fibrosis [32]. The perfusion of TGF-β2 into the anterior eye segment causes accumulation of fibrillary material in the TM [36], and elevated IOP and decreased AH outflow facility in a time-dependent manner, with increased fibronectin levels in the TM [27]. With regard to in vivo studies, sustained adenoviral overexpression of latent TGF-β2 induces ocular hypertension in rats and mice with statistically significantly

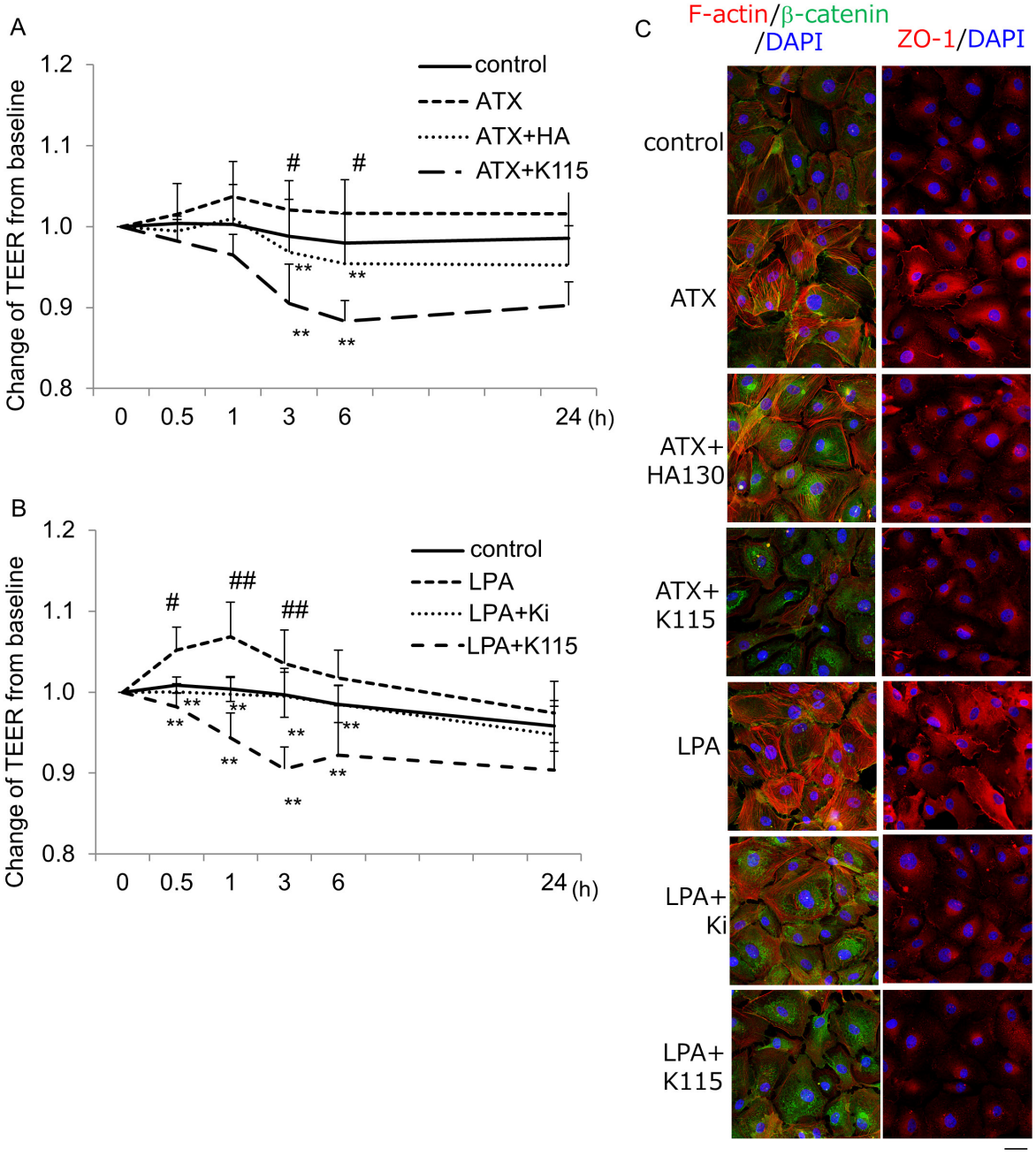

Figure 8. Effects of ATX and LPA on the TEER and molecules associated with cell–cell contact in SCE cells. **A**: The TEER measured in SCE cells exposed to ATX with or without the ATX inhibitor or ROCK inhibitor at 0.5, 1, 3, 6, and 24 h after treatment. Autotaxin (ATX) statistically significantly increased the transendothelial electrical resistance (TEER) at 3 and 6 h, and these effects were statistically significantly attenuated by the ATX inhibitor or ROCK inhibitor. **B**: The TEER measured in Schlemm's canal endothelial (SCE) cells exposed to lysophosphatidic acid (LPA) with or without the LPAR antagonist or the ROCK inhibitor at 0.5, 1, 3, 6, and 24 h after treatment. LPA statistically significantly increased the TEER at 0.5, 1, and 3 h, and these effects were statistically significantly attenuated by the LPAR antagonist or the ROCK inhibitor. Values are the mean ± standard deviation. (n = 4–9) $^{\#}p<0.05$, $^{\#\#}p<0.01$ normal versus ATX or LPA treatment; *p<0.05, **p<0.01 ATX or LPA treatment versus each treatment. **C**: Immunocytochemistry in SCE cells 3 h after treatment with ATX or LPA. The left panels show staining for F-actin (red) and β-catenin (green) merged with 4',6-diamidino-2-phenylindole (DAPI; blue). The right panels show staining for ZO-1 (red) merged with DAPI (blue). ATX and LPA induced rearrangement of F-actin, and upregulation of β-catenin and ZO-1 after treatment. These effects were statistically significantly attenuated by the ATX inhibitor, the LPAR antagonist, and the ROCK inhibitor. Bar, 200 µm.

reduced AH outflow facility after 4–7 days [13]. Thus, exogenous TGF-β2 is able to mimic the pathophysiology of POAG and cause IOP elevation. However, statistically significant effects of TGF-β2 on the IOP of perfused human anterior segments were observed after 24 h in a previous study [37]. In the present study, we examined the effects of TGF-β2 on fibrotic and cytoskeletal changes in TM cells and the permeability of SCE cells, and found that statistically significant fibrotic changes were induced by TGF-β2 within 24 h, which was confirmed with RT-qPCR and immunocytochemistry (Figure 2, Figure 3, and Figure 4), but the effects of TGF-β2 on SCE permeability were not statistically significant within 24 h. In addition, we observed significant IOP elevation 24 h after intracameral instillation of TGF-β2 (Figure 9), which was consistent with the previous report.

Although TGF -β1 has been suggested to have a pathological role in glaucoma based on the results of genetic analyses and its possible role in the pathology of IOP elevation mediated by fibrotic regulation of TM and ECM remodeling [38,39], it has been speculated that high IOP itself may induce the expression of activated TGF-β1 in TM cells, and the actual pathological role of TGF-β1 in glaucoma remains unclear [40]. We and other groups have reported that cytomegalovirus (CMV) infection induces statistically significant upregulation of TGF-β1 in hTM cells, which could be related to the enhanced fibrotic response in the TM [41-43]. However, ATX was also statistically significantly induced by CMV infection preceding upregulation of TGF-β1 in the TM, and TGF-β1 showed no correlation with IOP, while ATX showed a statistically significant positive correlation with IOP [43]. In the present study, cytoskeletal and fibrotic responses to TGF-β1 were observed with immunocytochemistry, but were weaker compared to those of TGF-β2 (Figure 4), and TGF-β1-induced mRNA upregulation was not statistically significant except α-SMA (Figure 3). TGF-β1 did not show any effects on SCE permeability. TGF-β1 may not play a statistically significant role in IOP elevation, although TGF-β1 may be involved in the pathogenesis of glaucomatous changes in the AH outflow pathway in the long-term, including TM fibrosis. Taken together, these results suggest that TGF-β2 is involved in glaucomatous changes in hTM cells, including cytoskeletal responses, EMT changes, and fibrogenic changes. In contrast, TGF-β1 may be partially involved in the pathogenesis of glaucoma, but not that statistically significantly involved compared to TGF-β2.

In previous studies that used AH samples obtained from patients with glaucoma, elevation of the ATX/LPA pathway was found in glaucomatous eyes, particularly in SOAG and XFG, subtypes of glaucoma in which the IOP often fluctuates and shows statistically significant increases [16]. In the same study, we also found statistically significant positive correlations between AH levels of ATX or LPA and IOP. The present results indicate that ATX and LPA induce significant fibrotic changes in hTM cells (Figures 6 and 7). Immunocytochemical analyses revealed that the fibrotic changes induced by LPA were more rapid than the changes induced by ATX (from 3 h after treatment versus after 6 h, respectively). Similar to the effects in hTM cells, LPA and ATX statistically significantly reduced SCE permeability as confirmed with the TEER, and statistically significantly upregulated ZO-1 and β-catenin expression (Figure 8). The TEER results also showed that the effects of LPA were seen more quickly than the effects of ATX (from 0.5 h after LPA treatment versus from 3 h after ATX treatment). However, the effects of LPA diminished promptly, while the effects of ATX were sustained until 24 h after treatment. As ATX is the enzyme responsible

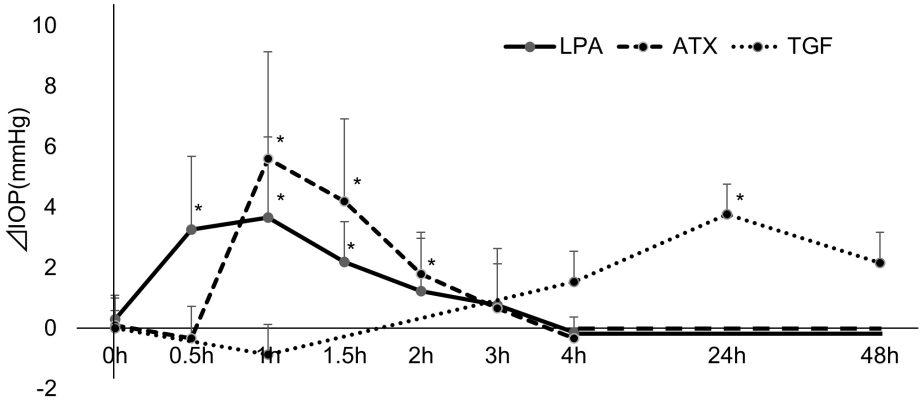

Figure 9. Effects of intracameral TGF-β2, ATX, and LPA on intraocular pressure in IOP of rabbit eyes was measured after intracameral instillation of 30 µl of 400 µM autotaxin (ATX), 100 µM lysophosphatidic acid (LPA), and 100 ng/ml TGF-β2 and compared to control eyes treated with PBS alone (control; n = 5). *p<0.05.

for generating LPA, this difference in timing and sustainability is reasonable. The intracameral instillation of ATX and LPA resulted in statistically significant IOP elevation in rabbit eyes, and we also observed a difference in the timing of the peak IOP elevation between ATX and LPA (Figure 9). Notably, the ATX/LPA pathway induced IOP elevation from as early as 0.5 h after treatment with LPA and 1 h after treatment with ATX, which were statistically significantly quicker than the effects of TGF-β2.

We reported previously that the inhibition of Rho-ROCK signaling induces changes in the cytoskeleton and focal adhesions in hTM cells, resulting in increased outflow facility and IOP reduction [44]. We have also reported that the inhibition of Rho-ROCK signaling results in Rho/ROCK-dependent cytoskeletal reorganization and disruption of proteins associated with tight junctions, leading to increased SCE permeability and increased AH outflow [25]. TGF-β2 and ATX/LPA are the upstream mediators of Rho-ROCK signaling, and in the present study, the ROCK inhibitor, K115, statistically significantly attenuated fibrotic changes in hTM cells induced by TGF-β2 or ATX/LPA. The ROCK inhibitor also statistically significantly attenuated the decreased SCE permeability induced by ATX/LPA. Therefore, it is possible that the altered Rho-ROCK signaling induced by TGF-β2 or ATX/LPA or both may play a role in the fibrotic changes in hTM cells or the decreased SCE permeability, but there were statistically significant differences in the timing of the effects, which may reflect the differences in upregulation of these mediators in different glaucoma subtypes.

The present study had several limitations. The observation periods were short, and we focused only on 24 h after treatment. Therefore, further studies with longer observation, including the investigation of the effects of TGF-β1, are required. We compared the cellular changes using hTM cells and SCE cells and found that the fibrotic change in the hTM cells and the decreased permeability in the SCE cells was induced by the mediators. Although it has been suggested that the decreased SCE permeability is associated with decreased AH outflow and IOP elevation, perfusion studies using enucleated eyes should be performed to examine the outflow facility and compare the morphological changes between TGF-β2- and ATX/LPA-treated eyes. In conclusion, TGF-β2 and ATX/LPA are involved in changes in fibrosis in hTM cells and cell–cell contact in SCE cells, and increases in the IOP, but the timing and sustainability differ between mediators, suggesting that they may play specific roles in different glaucoma subtypes.

ACKNOWLEDGMENTS

This work was supported by the Japan Society for the Promotion of Science (JSPS) Grant Number 15K10854 (MH), 20H03839 (MA). The English in this document has been checked by at least two professional editors, both native speakers of English. For a certificate, please see: Certificate. Conflict of interest statement: Shota Simizu is an employee of Senju Pharmaceutical Co. Ltd. Financial Support Supported by JSPS KAKENHI Grant Number 18K16946 (RY), 15K10854 (MH) and 20H03839 (MA).

REFERENCES

1. Quigley HA. Open-angle glaucoma. N Engl J Med 1993; 328:1097-106. [PMID: 8455668].
2. Gabelt BAT, Kaufman PL. Changes in aqueous humor dynamics with age and glaucoma. Prog Retin Eye Res 2005; 24:612-37. [PMID: 15919228].
3. Kwon YH, Fingert JH, Kuehn MH, Alward WL. Primary open-angle glaucoma. N Engl J Med 2009; 360:1113-24. [PMID: 19279343].
4. Honjo M, Tanihara H. Impact of the Clinical Use of ROCK Inhibitor on the Pathogenesis and Treatment of Glaucoma. Jpn J Ophthalmol 2018; 62:109-26. [PMID: 29445943].
5. Keller KE, Aga M, Bradley JM, Kelley MJ, Acott TS. Extracellular matrix turnover and outflow resistance. Exp Eye Res 2009; 88:676-82. [PMID: 19087875].
6. Vranka JA, Kelley MJ, Acott TS, Keller KE. Extracellular matrix in the trabecular meshwork: intraocular pressure regulation and dysregulation in glaucoma. Exp Eye Res 2015; 133:112-25. [PMID: 25819459].
7. Ikushima H, Miyazono K. Biology of transforming growth factor-β signaling. Curr Pharm Biotechnol 2010; 12:2099-107. [PMID: 21619537].
8. Moustakas A, Heldin CH. The regulation of TGFbeta signal transduction. Development 2009; 136:3699-714. [PMID: 19855013].
9. Jampel HD, Roche N, Stark WJ, Roberts AB. Transforming growth factor-β in human aqueous humor. Curr Eye Res 1990; 9:963-9. [PMID: 2276273].
10. Cousins SW, McCabe MM, Danielpour D. Identification of transforming growth factor-beta as an immunosuppressive factor in aqueous humor. Invest Ophthalmol Vis Sci 1991; 32:2201-11. [PMID: 2071334].
11. Shu DY, Lovicu FJ. Myofibroblast transdifferentiation: The dark force in ocular wound healing and fibrosis. Prog Retin Eye Res 2017; 60:44-65. [PMID: 28807717].
12. Zhu HJ, Burgess AW. Regulation of transforming growth factor-beta signaling. Mol Cell Biol Res Commun 2001; 4:321-30. [PMID: 11703090].
13. Shepard AR, Millar JC, Pang IH, Jacobson N, Wang WH, Clark AF. Adenoviral gene transfer of active human transforming

growth factor-beta2 elevates intraocular pressure and reduces outflow facility in rodent eyes. Invest Ophthalmol Vis Sci 2010; 51:2067-76. [PMID: 19959644].

14. Fleenor DL, Shepard AR, Hellberg PE, Jacobson N, Pang IH, Clark AF. TGF-beta2-induced changes in human trabecular meshwork: implications for intraocular pressure. Invest Ophthalmol Vis Sci 2006; 47:226-34. [PMID: 16384967].

15. Honjo M, Igarashi N, Nishida J, Kurano M, Yatomi Y, Igarashi K, Kano K, Aoki J, Aihara M. Role of the Autotaxin-LPA Pathway in Dexamethasone-Induced Fibrotic Responses and Extracellular Matrix Production in Human Trabecular Meshwork Cells. Invest Ophthalmol Vis Sci 2018; 59:21-30. [PMID: 29305605].

16. Honjo M, Igarashi N, Kurano M, Yatomi Y, Igarashi K, Kano K, Aoki J, Weinreb RN, Aihara M. Autotaxin-Lysophosphatidic Acid Pathway in Intraocular Pressure Regulation and Glaucoma Subtypes. Invest Ophthalmol Vis Sci 2018; 59:693-701. [PMID: 29392315].

17. Moolenaar WH, van Meeteren LA, Giepmans BN. The ins and outs of lysophosphatidic acid signaling. BioEssays 2004; 26:870-81. [PMID: 15273989].

18. Hama K, Aoki J, Fukaya M, Kishi Y, Sakai T, Suzuki R, Ohta H, Yamori T, Watanabe M, Chun J, Arai H. Lysophosphatidic acid and autotaxin stimulate cell motility of neoplastic and non-neoplastic cells through LPA1. J Biol Chem 2004; 279:17634-9. [PMID: 14744855].

19. Ho LTY, Skiba N, Ullmer C, Rao PV. Lysophosphatidic Acid Induces ECM Production via Activation of the Mechanosensitive YAP/TAZ Transcriptional Pathway in Trabecular Meshwork Cells. Invest Ophthalmol Vis Sci 2018; 59:1969-84. [PMID: 29677358].

20. Rao PV, Pattabiraman PP, Kopczynski C. Role of the Rho GTPase/Rho kinase signaling pathway in pathogenesis and treatment of glaucoma: Bench to bedside research. Exp Eye Res 2017; 15:23-32. [PMID: 27593914].

21. Mettu PS, Deng PF, Misra UK, Gawdi G, Epstein DL, Rao PV. Role of lysophospholipid growth factors in the modulation of aqueous humor outflow facility. Invest Ophthalmol Vis Sci 2004; 45:2263-71. [PMID: 15223804].

22. Keller KE, Bhattacharya SK, Borrás T, Brunner TM, Chansangpetch S, Clark AF, Dismuke WM, Du Y, Elliott MH, Ethier CR, Faralli JA, Freddo TF, Fuchshofer R, Giovingo M, Gong H, Gonzalez P, Huang A, Johnstone MA, Kaufman PL, Kelley MJ, Knepper PA, Kopczynski CC, Kuchtey JG, Kuchtey RW, Kuehn MH, Lieberman RL, Lin SC, Liton P, Liu Y, Lütjen-Drecoll E, Mao W, Masis-Solano M, McDonnell F, McDowell CM, Overby DR, Pattabiraman PP, Raghunathan VK, Rao PV, Rhee DJ, Chowdhury UR, Russell P, Samples JR, Schwartz D, Stubbs EB, Tamm ER, Tan JC, Toris CB, Torrejon KY, Vranka JA, Wirtz MK, Yorio T, Zhang J, Zode GS, Fautsch MP, Peters DM, Acott TS, Stamer WD. Consensus recommendations for trabecular meshwork cell isolation, characterization and culture. Exp Eye Res 2018; 171:164-73. [PMID: 29526795].

23. Stamer WD, Clark AF. The many faces of the trabecular meshwork cell. Exp Eye Res 2017; 158:112-23. d.[PMID: 27443500].

24. Zhu W, Cheyanne R. Godwin, Lin Cheng, Scheetz TE, Kuehn MH. Transplantation of iPSC-TM stimulates division of trabecular meshwork cells in human eyes Sci Rep 2020; 10:2905-[PMID: 32076077].

25. Kameda T, Inoue T, Inatani M, Fujimoto T, Honjo M, Kasaoka N, Inoue-Mochita M, Yoshimura N, Tanihara H. The effect of Rho-associated protein kinase inhibitor on monkey Schlemm's canal endothelial cells. Invest Ophthalmol Vis Sci 2012; 53:3092-103. [PMID: 22491412].

26. Underwood JL, Murphy CG, Chen J. Glucocorticoids regulate transendothelial fluid flow resistance and formation of intercellular junctions. Am J Physiol Cell Physiol 1999; 277:C330-42. [PMID: 10444410].

27. Alvarado JA, Betanzos A, Franse-Carman L, Chen J, Gonzalez-Mariscal L. Endothelia of Schlemm's canal and trabecular meshwork: distinct molecular, functional, and anatomic features. Am J Physiol Cell Physiol 2004; 286:C621-34. [PMID: 14613887].

28. Igarashi N, Honjo M, Kurano M, Yatomi Y, Igarashi K, Kano K, Aoki J, Aihara M. Increased aqueous autotaxin and lysophosphatidic acid levels are potential prognostic factors after trabeculectomy in different types of glaucoma. Sci Rep 2018; 8:11304-[PMID: 30054520].

29. Fujimoto T, Inoue T, Kameda T, Kasaoka N, Inoue-Mochita M, Tsuboi N, Tanihara H. Involvement of RhoA/Rho-associated kinase signal transduction pathway in dexamethasone-induced alterations in aqueous outflow. Invest Ophthalmol Vis Sci 2012; 53:7097-08. [PMID: 22969074].

30. Birke MT, Birke K, Lutjen-Drecoll E, Schlotzer-Schrehardt U, Hammer CM. Cytokine-dependent ELAM-1 induction and concomitant intraocular pressure regulation in porcine anterior eye perfusion culture. Invest Ophthalmol Vis Sci 2011; 52:468-75. [PMID: 20861478].

31. Tsuboi N, Inoue T, Kawai M, Inoue-Mochita M, Fujimoto T, Awai-Kasaoka N, Tanihara H. The effect of monocyte chemoattractant protein-1/CC chemokine ligand 2 on aqueous humor outflow facility. Invest Ophthalmol Vis Sci 2012; 53:6702-7. [PMID: 22956618].

32. Stamer WD, Acott TS. Current understanding of conventional outflow dysfunction in glaucoma. Curr Opin Ophthalmol 2012; 23:135-43. [PMID: 22262082].

33. Inatani M, Tanihara H, Katsuta H, Honjo M, Kido N, Honda Y. Transforming growth factor-beta 2 levels in aqueous humor of glaucomatous eyes. Graefes Arch Clin Exp Ophthalmol 2001; 239:109-13. [PMID: 11372538].

34. Picht G, Welge-Luessen U, Grehn F, Lütjen-Drecoll E. Transforming growth factor beta 2 levels in the aqueous humor in different types of glaucoma and the relation to filtering bleb development. Graefes Arch Clin Exp Ophthalmol 2001; 239:199-207. [PMID: 11405069].

35. Guo T, Guo L, Fan Y, Fang L, Wei J, Tan Y, Chen Y, Fan X. Aqueous humor levels of TGFβ2 and SFRP1 in different types of glaucoma. BMC Ophthalmol 2019; 19:170-[PMID: 31382918].

36. Gottanka J, Chan D, Eichhorn M, Lütjen-Drecoll E, Ethier CR. Effects of TGF-beta2 in perfused human eyes. Invest Ophthalmol Vis Sci 2004; 45:153-8. [PMID: 14691167].

37. Fleenor DL, Shepard AR, Hellberg PE, Jacobson N, Pang IH, Clark AF. TGFβ2-induced changes in human trabecular meshwork: Implications for intraocular pressure. Invest Ophthalmol Vis Sci 2006; 47:226-34. [PMID: 16384967].

38. Danford ID, Verkuil LD, Choi DJ, Collins DW, Gudiseva HV, Uyhazi KE, Lau MK, Kanu LN, Grant GR, Chavali VRM, O'Brien JM. Characterizing the "POAGome": A bioinformatics-driven approach to primary open-angle glaucoma. Prog Retin Eye Res 2017; 58:89-114. [PMID: 28223208].

39. Hill LJ, Mead B, Thomas CN, Foale S, Feinstein E, Berry M, Blanch RJ, Ahmed Z, Logan A. TGF-β-induced IOP elevations are mediated by RhoA in the early but not the late fibrotic phase of open angle glaucoma. Mol Vis 2018; 24:712-26. [PMID: 30429640].

40. Kirwan RP, Crean JK, Fenerty CH, Clark AF, O'Brien CJ. Effect of cyclical mechanical stretch and exogenous transforming growth factor-beta1 on matrix metalloproteinase-2 activity in lamina cribrosa cells from the human optic nerve head. J Glaucoma 2004; 13:327-34. [PMID: 15226662].

41. Choi JA, Kim JE, Noh SJ, Kyoung Kim E, Park CK, Paik SY. Enhanced cytomegalovirus infection in human trabecular meshwork cells and its implication in glaucoma pathogenesis. Sci Rep 2017; 7:43349-[PMID: 28240260].

42. Choi JA, Kim JE, Ju HH, Lee J, Jee D, Park CK, Paik SY. The effects of losartan on cytomegalovirus infection in human trabecular meshwork cells. PLoS One 2019; 14:e0218471-[PMID: 31216320].

43. Igarashi N, Honjo M, Yamagishi R, Kurano M, Yatomi Y, Igarashi K, Kaburaki T, Aihara M. Involvement of autotaxin in the pathophysiology of elevated intraocular pressure in Posner-Schlossman syndrome. Sci Rep 2020; 10:6265-[PMID: 32286414].

44. Honjo M, Tanihara H, Inatani M, Kido N, Sawamura T, Yue BY, Narumiya S, Honda Y. Effects of rho-associated protein kinase inhibitor Y-27632 on intraocular pressure and outflow facility. Invest Ophthalmol Vis Sci 2001; 42:137-44. [PMID: 11133858].

Articles are provided courtesy of Emory University and the Zhongshan Ophthalmic Center, Sun Yat-sen University, P.R. China. The print version of this article was created on 20 January 2021. This reflects all typographical corrections and errata to the article through that date. Details of any changes may be found in the online version of the article.